

Rapidly rotating black holes in dynamical Chern-Simons gravity: Decoupling limit solutions and breakdown

Leo C. Stein*

Center for Radiophysics and Space Research, Cornell University, Ithaca, NY 14853, USA

(Dated: 22 August 2014)

Rapidly rotating black holes are a prime arena for understanding corrections to Einstein's theory of general relativity (GR). We construct solutions for rapidly rotating black holes in dynamical Chern-Simons (dCS) gravity, a useful and motivated example of a post-GR correction. We treat dCS as an effective theory and thus work in the decoupling limit, where we apply a perturbation scheme using the Kerr metric as the background solution. Using the solutions to the scalar field and the trace of the metric perturbation, we determine the regime of validity of our perturbative approach. We find that the maximal spin limit may be divergent, and the decoupling limit is strongly restricted for rapid rotation. Rapidly-rotating stellar-mass BHs can potentially be used to place strong bounds on the coupling parameter ℓ of dCS. In order for the black hole observed in GRO J1655-40 to be within the decoupling limit we need $\ell \lesssim 22$ km, a value 7 orders of magnitude smaller than present Solar System bounds on dynamical Chern-Simons gravity.

PACS numbers: 04.50.Kd, 04.25.dg, 04.25.-g

I. INTRODUCTION

General relativity (GR), despite its tremendous experimental and observational success [1], is widely believed to be incomplete. GR is the only classical (non-quantum) sector of our description of nature. Semi-classical studies suggest that the confrontation between gravity and quantum mechanics leads to new physics [2–4], perhaps at the Planck scale.

Fundamental (top-down) approaches to a quantum resolution include string theory and loop quantum gravity, though these approaches may be as misguided as attempting to canonically quantize sound waves [5]. The bottom-up alternative is to explore what *effective* theories may arise from more fundamental ones, and look for the phenomenology they predict. To this end there are several well-motivated and studied corrections to GR, such as scalar-tensor theories [6], Einstein-dilaton-Gauss-Bonnet (EdGB) [7], and new massive gravity [8]. In this paper we focus on dynamical Chern-Simons (dCS) gravity [9, 10], which is motivated from anomaly cancellation in QFT, the low-energy limit of string theories, or simply by being the lowest-order parity-odd gravitational interaction. The phenomenology of dCS is different from other low-order corrections because it is parity-odd.

Almost all corrections to GR, including dCS, involve a dimensional coupling constant ℓ , i.e. an explicit length (or inverse energy) scale. It is this length scale ℓ which we want to measure or observationally bound. The length scale can not be too long, otherwise we might have already noticed deviations in the weak-field (long curvature radius) where GR is an excellent description. This motivates a perturbative expansion in powers of the dimensionless ratio (ℓ/\mathcal{R}) , with \mathcal{R} a background length scale. This is

called the decoupling limit or weak-coupling expansion, and the leading order equations and solutions are those of GR. In the weak-coupling regime the theory is approximately well-posed, even if it is not well-posed as an exact theory [11].

In this paper we study the regime of validity of the decoupling limit in dCS by examining numerical solutions about rotating BHs, presented in Figure 1. Rapidly-rotating stellar-mass BHs achieve some of the highest-curvature gravitational fields in the present universe. As the mass decreases and as the rotation of a BH increases, the event horizon moves inward and the horizon curvature grows. Thus rapidly-rotating stellar-mass BHs are a natural place to look to understand GR or to exper-

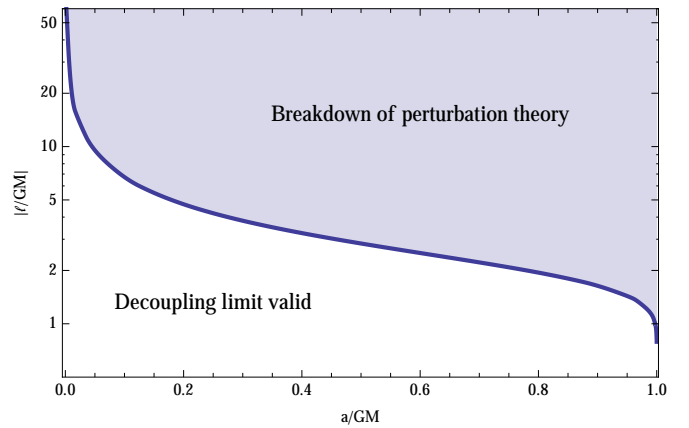


FIG. 1. (Color online) The regime of validity of the perturbation theory in the (spin, coupling strength) plane. The perturbation scheme is not controlled in the shaded (upper) region. The small- a behaviour can be understood analytically as $|\ell/GM| \lesssim \mathcal{O}(a^{-1/2})$. At any ℓ , the Chern-Simons correction becomes more important at higher spin, and the perturbation scheme eventually breaks down. The separatrix comes from Eq. (26), $|\ell/GM|^4 = 1/\max|\tilde{h}(a/GM)|$.

* Einstein fellow; leostein@astro.cornell.edu

imentally probe for the presence of corrections to GR. These BHs provide the strictest limits on the applicability of the weak-coupling expansion. Present rotating BH solutions in dCS are all in the slow-rotation limit [12–15], so here we extend to rapid rotation by constructing numerical solutions. This is similar to what has been done in Ref. [16], who did not study the validity of the weak-coupling expansion, and in Ref. [17] for EdGB.

The plan for this paper is as follows. In Sec. II we specify the action, lay out the equations of motion for dCS, and develop the equations in the decoupling limit. We pay special attention to the trace of the metric deformation, which is simpler than the full problem, yet allows us to determine the validity of the perturbation scheme. In Sec. III we specialize to the Kerr background geometry and rescale our functions of interest to make the ℓ dependence explicit. In Sec. IV we describe our numerical scheme and the properties of the solutions. Finally in Sec. V we interpret the solutions, determining the regime of validity, and report what present BH observations can say about ℓ .

II. ACTION, EQUATIONS OF MOTION, AND DECOUPLING LIMIT

We work in units where $c = 1 = \hbar$ so that $[M] = [L]^{-1}$, metric signature $(-1, +1, +1, +1)$, and the sign conventions of Wald [18]. We take as our action

$$S = \int d^4x \sqrt{-g} [L_{\text{EH}} + L_{\vartheta} + L_{\text{int}}] \quad (1)$$

with

$$L_{\text{EH}} = \frac{m_{\text{pl}}^2}{2} R, \quad L_{\vartheta} = \frac{-1}{2} (\partial\vartheta)^2, \quad L_{\text{int}} = \frac{m_{\text{pl}}}{8} \ell^2 \vartheta *RR. \quad (2)$$

Here R is the Ricci scalar of the metric g_{ab} , with determinant g , and the reduced Planck mass satisfies $m_{\text{pl}}^2 = (8\pi G)^{-1}$. The axionic field ϑ has been canonically normalized and so has dimensions $[\vartheta] = [L]^{-1}$. In the interaction term we see the Pontryagin-Chern density

$$*RR = -*R^{abcd}R_{abcd} = -\frac{1}{2}\epsilon^{abef}R_{ef}{}^{cd}R_{abcd} \quad (3)$$

which is the lowest-order parity-odd curvature invariant, constructed from the Riemann tensor R_{abcd} and the Levi-Civita tensor ϵ^{abcd} . $*RR$ is also a topological invariant, i.e. the integral $\int *RR\sqrt{-g}d^4x$ depends only on the topology of the manifold. Finally we also have the length scale ℓ which relates to the length at which this non-minimal interaction term becomes important. ℓ can be thought of as a dimensional coupling coefficient. In the limit $\ell \rightarrow 0$, general relativity is recovered. It is this length scale ℓ which in principle could be observationally constrained.

Variation of this action with respect to ϑ leads to the scalar equation of motion

$$\square\vartheta = -\frac{m_{\text{pl}}}{8}\ell^2 *RR, \quad (4)$$

where $\square = \nabla^a\nabla_a$ and ∇_a is the covariant derivative compatible with the metric. Variation of the action with respect to the inverse metric g^{ab} leads to the metric equation of motion

$$m_{\text{pl}}^2 G_{ab} + m_{\text{pl}}\ell^2 C_{ab} = T_{ab}^{(m)} + T_{ab}^{(\vartheta)}. \quad (5)$$

Here we have the stress-energy tensor of any matter fields, $T_{ab}^{(m)}$, and the stress-energy tensor of the canonical scalar with flat potential,

$$T_{ab}^{(\vartheta)} = \nabla_a\vartheta\nabla_b\vartheta - \frac{1}{2}g_{ab}\nabla^c\vartheta\nabla_c\vartheta. \quad (6)$$

We also have the C -tensor, with the convention [10] (hence the factor of $\frac{1}{8}$ in the action)

$$C_{ab} = \epsilon^{cde}{}_{(a}R_{b)c;d}\vartheta_{;e} + *R^c{}_{(ab)}{}^d\vartheta_{;cd}. \quad (7)$$

The C -tensor is trace-free, $g^{ab}C_{ab} = 0$, and it satisfies the divergence identity

$$\nabla^a \left(T_{ab}^{(\vartheta)} - m_{\text{pl}}\ell^2 C_{ab} \right) = \left(\square\vartheta + \frac{m_{\text{pl}}}{8}\ell^2 *RR \right) \nabla_b\vartheta = 0. \quad (8)$$

Thus we have ordinary conservation of matter stress-energy, $\nabla^a T_{ab}^{(m)} = 0$. In this paper we will not consider any matter sources, $T_{ab}^{(m)} = 0$.

We now take the decoupling limit, where we assume that the corrections due to the interaction term are ‘‘small.’’ This allows us to perform a controlled, perturbative expansion of all the fields in terms of the coupling strength ℓ . We will introduce a formal order-counting parameter ε to keep track of the perturbation scheme, which can be set to 1 later, which counts the order in ℓ^2 . That is, we take $\ell^2 \rightarrow \varepsilon\ell^2$ and expand both the metric and scalar in powers of ε : $\vartheta = \sum_{k=0}^{\infty} \varepsilon^k \vartheta^{(k)}/k!$ and similarly for the metric. In order to recover the GR solution in the limit $\varepsilon \rightarrow 0$, we have that $\vartheta^{(0)} = 0$, and $g_{ab}^{(0)} = g_{ab}^{\text{GR}}$ for some known solution.

From Eq. (4), we can see that the leading order solution for ϑ is $\vartheta^{(1)}$, which satisfies

$$\square^{(0)}\vartheta^{(1)} = -\frac{m_{\text{pl}}}{8}\ell^2 *RR^{(0)}. \quad (9)$$

From here forward we will drop the superscript (0) when it is unambiguous. Now analyze Eq. (5) with $\ell^2 \rightarrow \varepsilon\ell^2$, and recall that C_{ab} is linear in ϑ , while $T_{ab}^{(\vartheta)}$ is quadratic in ϑ . This shows that $h_{ab}^{(1)}$ has vanishing source term, and the leading order metric deformation away from GR enters at ε^2 : $g_{ab} = g_{ab}^{\text{GR}} + \varepsilon^2 h_{ab}^{(2)}/2 + \mathcal{O}(\varepsilon^3)$. We label this as $h_{ab}^{(2)}/2 \equiv h_{ab}^{\text{def}}$, which satisfies

$$m_{\text{pl}}^2 G_{ab}^{(1)}[h_{cd}^{\text{def}}] + m_{\text{pl}}\ell^2 C_{ab}[\vartheta^{(1)}] = T_{ab}^{(\vartheta)}[\vartheta^{(1)}, \vartheta^{(1)}], \quad (10)$$

where $G_{ab}^{(1)}[h_{cd}]$ is the linearized Einstein operator acting on the metric perturbation h_{cd} .

Our main concern in this paper is the regime of validity of the decoupling limit via this perturbation scheme.

To quantify if this scheme is under control, we must check that some appropriate dimensionless quantities are “small.” For example, in [19] it was possible to make scaling arguments for the ratio of the interaction Lagrangian L_{int} and the Einstein-Hilbert Lagrangian L_{EH} when in the presence of a matter source. However, this is not possible here because we are dealing with a matter-free background solution, so the E-H Lagrangian identically vanishes. Similarly, we can not make a comparison of $T_{ab}^{(\vartheta)}$ to G_{ab} , because matter-free backgrounds give a vanishing Einstein tensor. Instead, we investigate what is possible with the metric deformation h_{ab}^{def} .

Clearly it is much harder to solve the metric deformation equation (10) than the scalar equation Eq. (9). We will not attempt to solve for a full metric tensor deformation solution. Rather, note what is possible when tracing (with g_{GR}^{ab}) the metric deformation equation. With a Ricci-flat background and in the Lorenz gauge ($\nabla^b h_{ab}^{\text{def}} = \frac{1}{2}\nabla_a h^{\text{def}}$) we find

$$\frac{1}{2}m_{\text{pl}}^2\Box h^{\text{def}} = -(\nabla^a\vartheta^{(1)})(\nabla_a\vartheta^{(1)}), \quad (11)$$

where $h^{\text{def}} = g_{\text{GR}}^{ab}h_{ab}^{\text{def}}$ is the trace of the metric perturbation. This is just another sourced scalar d’Alembertian equation, the same type of equation we must solve for the the scalar field $\vartheta^{(1)}$.

Once we find a solution for h^{def} , we still have to find an appropriate dimensionless comparison in order to verify that the perturbation scheme is under control. Consider the perturbative expansion of the volume element:

$$\sqrt{-g} = \sqrt{-g^{\text{GR}}}(1 + \varepsilon^2\frac{1}{2}h^{\text{def}}) + \mathcal{O}(\varepsilon^3). \quad (12)$$

If the quantity h^{def} becomes $\mathcal{O}(1)$, then clearly we should keep higher order terms in this expansion. Although this statement is gauge-dependent, it gives an order of magnitude estimate of the regime of validity of the perturbation scheme. There are also gauge-invariant quantities that can be constructed from h^{def} , such as the perturbed 4-volume of a region. Moreover, the BH-spin-dependent structure of the regime of validity will still be revealed with this condition. Therefore we define our criterion for the perturbation to be under control:

$$|h^{\text{def}}| \lesssim 1. \quad (13)$$

III. KERR, SYMMETRY REDUCTION, AND SCALING

We are seeking rapidly rotating black hole solutions, and we have the luxury that at $\mathcal{O}(\varepsilon^0)$ our solution reduces to the one in GR. Therefore we take the Kerr metric, $g_{ab}^{\text{GR}} = g_{ab}^{\text{K}}$, which in Boyer-Lindquist coordinates is [18]

$$g_{ab}^{\text{K}}dx^a dx^b = -\frac{\Delta}{\Sigma}(dt - a\sin^2\theta d\phi)^2 + \Sigma\left(\frac{dr^2}{\Delta} + d\theta^2\right) + \frac{\sin^2\theta}{\Sigma}\left((r^2 + a^2)d\phi - a dt\right)^2, \quad (14)$$

with the total mass M , angular momentum per unit mass $a = J/M$ (with units $[a] = [L]$), $-GM < a < +GM$, and where

$$\Sigma \equiv r^2 + a^2 \cos^2\theta \quad (15)$$

$$\Delta \equiv r^2 + a^2 - 2GM r. \quad (16)$$

The event horizon is at the outer root r_+ of $\Delta = 0$, given by $r_{\pm} = GM \pm \sqrt{(GM)^2 - a^2}$. In these coordinates the root of the metric determinant is given by

$$\sqrt{-g^{\text{K}}} = \Sigma \sin\theta. \quad (17)$$

A straightforward calculation gives

$${}^*RR = 96(GM)^2 \frac{a\mu r(3r^2 - a^2\mu^2)(r^2 - 3a^2\mu^2)}{\Sigma^6}, \quad (18)$$

where we use the shorthand $\mu = \cos\theta$.

The d’Alembertian operator \Box in the Kerr background is somewhat complicated, but since we are seeking stationary and axisymmetric solutions, the operator simplifies:

$$\Box f(r, \theta) = \frac{1}{\sqrt{-g}}\partial_a(\sqrt{-g}g^{ab}\partial_b f(r, \theta)), \quad (19)$$

$$\Sigma\Box f(r, \theta) = [\partial_r\Delta\partial_r + \partial_\mu(1 - \mu^2)\partial_\mu]f, \quad (20)$$

where $\partial_\mu = \frac{\partial}{\partial \cos\theta} = \frac{-1}{\sin\theta}\frac{\partial}{\partial\theta}$.

Before discussing how to solve this partial differential equation (PDE), let us rescale to dimensionless coordinates, which will also elucidate the mass dependence of the solution. Let $\tilde{r} \equiv r/GM$, $\tilde{a} \equiv a/GM$, $\tilde{\Delta} \equiv \Delta/(GM)^2 = \tilde{r}^2 + \tilde{a}^2 - 2\tilde{r}$, $\tilde{\Sigma} \equiv \Sigma/(GM)^2 = \tilde{r}^2 + \tilde{a}^2\mu^2$. Analyzing the equation of motion for $\vartheta^{(1)}$ we find that we should rescale it as

$$\vartheta^{(1)} = \tilde{\vartheta}m_{\text{pl}}\frac{\ell^2}{(GM)^2}. \quad (21)$$

Then the equation for $\tilde{\vartheta}$ is

$$\left[\partial_{\tilde{r}}\tilde{\Delta}\partial_{\tilde{r}} + \partial_\mu(1 - \mu^2)\partial_\mu\right]\tilde{\vartheta} = -12\frac{\tilde{a}\mu\tilde{r}(3\tilde{r}^2 - \tilde{a}^2\mu^2)(\tilde{r}^2 - 3\tilde{a}^2\mu^2)}{\tilde{\Sigma}^5}. \quad (22)$$

From the scaling in Eq. (21) we see some obvious features. As ℓ increases, $\vartheta^{(1)}$ increases, which is easy to understand since ℓ is acting as a coupling strength. We also see that black holes with lighter masses generate larger values of $\vartheta^{(1)}$. That is, the CS interaction is a higher-curvature operator, which is important at shorter lengths, which corresponds to lighter black holes. In other words, the curvature at the horizon of a black hole goes as $1/M^2$, so the greatest effect comes from the lightest black hole.

Now we perform another scaling analysis in the equation for h^{def} , Eq. (11). What we find is that we should introduce the scaling

$$h^{\text{def}} = \tilde{h}\left(\frac{\ell}{GM}\right)^4, \quad (23)$$

where \tilde{h} satisfies

$$\left[\partial_{\tilde{r}} \tilde{\Delta} \partial_{\tilde{r}} + \partial_{\mu} (1 - \mu^2) \partial_{\mu} \right] \tilde{h} = -2 \left[\tilde{\Delta} (\partial_{\tilde{r}} \tilde{\vartheta})^2 + (1 - \mu^2) (\partial_{\mu} \tilde{\vartheta})^2 \right]. \quad (24)$$

We again see that as ℓ increases and/or M decreases, h^{def} increases. In terms of the scaled variable \tilde{h} , the validity condition [Eq. (13)] reads

$$\left| \tilde{h} \left(\frac{\ell}{GM} \right)^4 \right| \lesssim 1. \quad (25)$$

Alternatively, if a black hole with some known spin \tilde{a} is found to be well-described everywhere by GR, we may claim the condition

$$\left| \frac{\ell}{GM} \right|^4 \lesssim \frac{1}{\max |\tilde{h}(\tilde{a})|}. \quad (26)$$

From this we see that lighter black holes will produce better bounds on ℓ , as will more rapidly-rotating black holes. This latter point comes from noting that in the small \tilde{a} expansion, $\tilde{h} \sim \mathcal{O}(\tilde{a}^2)$; thus more rapidly spinning black holes source a larger metric deformation and provide a more stringent bound on ℓ . Our goal now is to determine $\max |\tilde{h}(\tilde{a})|$ by solving the system comprising Eqs. (22) and (24).

IV. NUMERICAL SCHEME AND SOLUTIONS

Several approaches are available to try to solve the system of equations. Each equation is an elliptic PDE on the exterior domain $\tilde{r} \in [\tilde{r}_+, +\infty)$, $\mu \in [-1, +1]$. The factor of $\tilde{\Delta}$ in the $\partial_{\tilde{r}}^2$ goes to zero as $\tilde{r} \rightarrow \tilde{r}_+$, and the equation changes from an elliptic to a hyperbolic one inside the (outer) event horizon.

The first approach to solving this system was made in [20] for $\vartheta^{(1)}$ and [12, 13] for h_{ab}^{def} , by expanding all fields in a bivariate expansion in ε and a and finding the leading (linear in a) solution. This was further extended in [15] to quadratic order in a . However, we are interested in the full behaviour in a , not just a slow-rotation expansion. There is no guarantee that an expansion about $a = 0$ will converge as $\tilde{a} \rightarrow 1$. In fact, our numerical results will suggest that the $\tilde{a} \rightarrow 1$ limit is singular, which restricts the radius of convergence of an a expansion.

The wave equation on the Kerr background is amenable to separation of variables, as was demonstrated in the celebrated work of Teukolsky [21–23]. That feature is naturally retained here, and in terms of the separation approach, these solutions would have support only for vanishing temporal Fourier frequency $\omega = 0$ (stationary) and azimuthal number $m = 0$ (axisymmetric). This approach has recently been attempted by Konno and Takahashi [16]. In the separation of variables approach, the angular basis functions are simply Legendre polynomials $P_j(\mu)$; both

the source terms and solutions are expanded in this basis. It is straightforward to see that the solution for $\vartheta^{(1)}$ will have support only at odd j , while the solution for h^{def} has support only at even j . Konno and Takahashi gave formulae for the moments of the source Σ^*RR as a quadruple sum by expanding everything in powers of μ . Using a different approach, this author has presented a more compact form [24] in terms of rational polynomials of r times hypergeometric functions. These moments would then have to be integrated against the homogeneous solutions to the radial ODE for each mode. These homogeneous solutions are Legendre functions of the first and second kind, respectively $P_j(\eta)$ and $Q_j(\eta)$, where

$$\eta \equiv (r - GM)/b, \quad b = \sqrt{(GM)^2 - a^2}, \quad (27)$$

with $\eta \in [+1, +\infty)$. However, neither Konno and Takahashi nor the present author have found general expressions for the radial indefinite integrals.

Yet another analytic approach is to try to integrate the source term against the analytically known Green's function [25]. However, the Green's function is written in terms of a complete elliptic integral of the first kind [26], and the present author has not had any success integrating the source against the Green's function. We are unaware of any such attempt in the literature.

Instead, we solve the system of equations numerically. Still there are several approaches available. One may use a hyperbolic (wave equation) solver with some initial guess and just wait for the transient solution to settle down to the stationary one. Alternatively, one may use a relaxation scheme to solve the purely elliptic problem. In between these two approaches, one may add a $-\partial_t \tilde{\vartheta}$ term to the elliptic operator to make it parabolic, thus approximating an exponentially convergent relaxation scheme. All of these approaches are workable.

We will take advantage of the separability of our equation in order to directly invert the differential operator. This is the numerical analog of the Green's function approach, but applied mode-by-mode in the spectral decomposition.

Consider the same differential operator with any given source term,

$$\left[\partial_{\tilde{r}} \tilde{\Delta} \partial_{\tilde{r}} + \partial_{\mu} (1 - \mu^2) \partial_{\mu} \right] f = S. \quad (28)$$

Now expand both the source term S and the solution we seek f in terms of Legendre polynomials,

$$S(\tilde{r}, \mu) = \sum_{j=0}^{\infty} S_j(\tilde{r}) P_j(\mu), \quad (29)$$

where

$$S_j(\tilde{r}) = \frac{2j+1}{2} \int_{-1}^{+1} S(\tilde{r}, \mu) P_j(\mu) d\mu \quad (30)$$

and similarly for f , with the prefactor arising from the normalization

$$\int_{-1}^{+1} P_j(\mu) P_{j'}(\mu) d\mu = \frac{2}{2j+1} \delta_{jj'}. \quad (31)$$

This defines the forward and backward spectral transformation for the angular direction of the domain.

Now each f_j satisfies an ODE,

$$\left[\partial_{\tilde{r}} \tilde{\Delta} \partial_{\tilde{r}} - j(j+1) \right] f_j(\tilde{r}) = S_j(\tilde{r}). \quad (32)$$

We use a pseudospectral collocation scheme [27] to directly invert the differential operator appearing here. First, we remap the radial domain, using the definition of the dimensionless η [Eq. (27)], so that the radial domain is a -independent. Then we compactify via

$$\eta = \frac{2}{1-x}, \quad (33)$$

so that $x \in [-1, +1]$ with the horizon at $x = -1$ and spatial infinity at $x = +1$. In terms of this new radial coordinate, we have

$$\left[\frac{1}{4}(1-x)^2 \partial_x (3-x)(1+x) \partial_x - j(j+1) \right] f_j(x) = S_j(x). \quad (34)$$

Besides being compact, this coordinate has another advantage: the radial operator which we want to invert is now a -independent, which means the same solver [e.g. a lower-upper (LU) decomposition] can be precomputed once and applied for all a . Now we use Chebyshev polynomials as basis functions and the interior (“roots”) grid for the collocation points for our pseudospectral method [27] when solving Eq. (34).

The physical boundary conditions are regularity at both the horizon and infinity, which means that $\tilde{\vartheta}$ and \tilde{h} must vanish at $x = +1$. Recall that the homogeneous solutions (which comprise the null space of the full differential operator) are $P_j(\eta)$ and $Q_j(\eta)$. Since these blow up at one endpoint, they are automatically excluded by the discretized scheme (i.e. the discretized differential operator is full rank), except for $P_0(\eta)$. Therefore we must include one numerical boundary condition for the $j = 0$ mode to enforce vanishing at $x = +1$.

For the highest spins we have investigated, $\tilde{a} = 0.99995$, we have found that 55 angular basis functions and 64 radial grid points are sufficient to recover $\tilde{h}(x, \mu)$ with fractional errors estimated at the relative 3×10^{-8} level. Meanwhile, this resolution recovers solutions at lower spins (below $\tilde{a} \lesssim 0.998$) at the relative 3×10^{-12} level. Thus each j mode requires solving a linear system whose dimension is just 64. This scheme is implemented in MATHEMATICA, and solves for $\tilde{\vartheta}$ and \tilde{h} for a single value of \tilde{a} in 0.19 sec on a laptop computer.

The distribution of power into the P_j modes, as a function of the spin \tilde{a} , is seen in Fig. 2. For each solution $\tilde{\vartheta}_j(x)$ at a given spin, we plot a discrete estimate of the L^2 norm,

$$\left\| \tilde{\vartheta}_j(x) \right\|_2 = \int_{-1}^{+1} |\tilde{\vartheta}_j(x)|^2 dx. \quad (35)$$

For the odd function $\tilde{\vartheta}$, we only plot the power in odd j coefficients. The plot for the even function \tilde{h} looks

similar, when keeping just the even j 's. As expected, there is exponential convergence in P_j coefficients, because the sources and solutions are C^∞ . However, there is a striking feature in the spin-dependence of this exponential convergence. As spin increases, the rate of convergence decreases: more P_j coefficients are needed for the same accuracy. Finally, at sufficiently high \tilde{a} , the peak power is no longer in $\tilde{\vartheta}_1$, as can be seen in the line for $\tilde{a} = 0.999$.

Next we look at the spatial structure of some of the solutions in Fig. 3. The solutions are azimuthally symmetric, so we plot only a longitudinal section, with color corresponding to the value of the field (notice that the color scale differs for each panel). In the $(\tilde{r} \sin \theta, \tilde{r} \cos \theta)$ coordinates we use, the horizon is simply a circle (these are not the quasi-Cartesian Kerr-Schild coordinates, so they do not show the oblateness of the spacetime). The contours of constant field value (linearly spaced) help to highlight the multipole structure. The high multipole content is easily seen in the top-right panel.

We care most about the spin-dependence of $\max |\tilde{h}(\tilde{a})|$. As we can see in the bottom row of Fig. 3, \tilde{h} always attains its peak value on the horizon, at the equator ($\cos \theta = 0$). Because of the very strong radial dependence of the solution, this is difficult to see in the color density plots. It is made more apparent in the 3D surface plot of Fig. 4. There we use the same $(\tilde{r} \sin \theta, \tilde{r} \cos \theta)$ coordinates for the horizontal directions, and turn the field value of \tilde{h} into the vertical height of the surface. We have plotted the solution for $\tilde{a} = 0.99$, but the qualitative structure is similar for other spins: the peak value is at the horizon, on the equator.

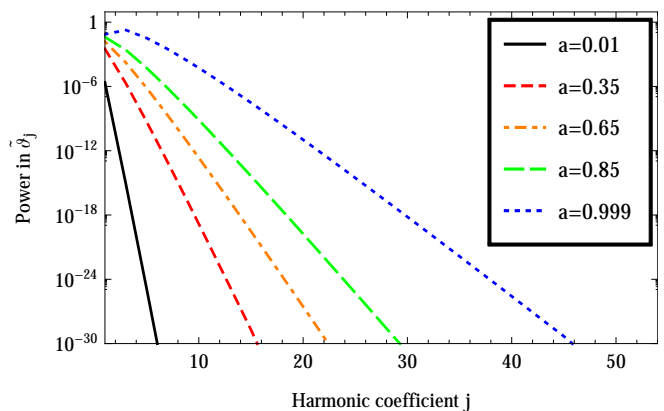


FIG. 2. (Color online) Smooth solutions for $\tilde{\vartheta}$ and \tilde{h} have exponential convergence as a decomposition in Legendre polynomials $P_j(\cos \theta)$. The vertical axis is the L^2 norm of $\tilde{\vartheta}_j(x)$ [Eq. (35)]. At low spin, the convergence is more rapid, and few coefficients are needed. As spin increases more coefficients must be kept. Only the odd coefficients of $\tilde{\vartheta}$ are plotted. \tilde{h} follows the same trend.

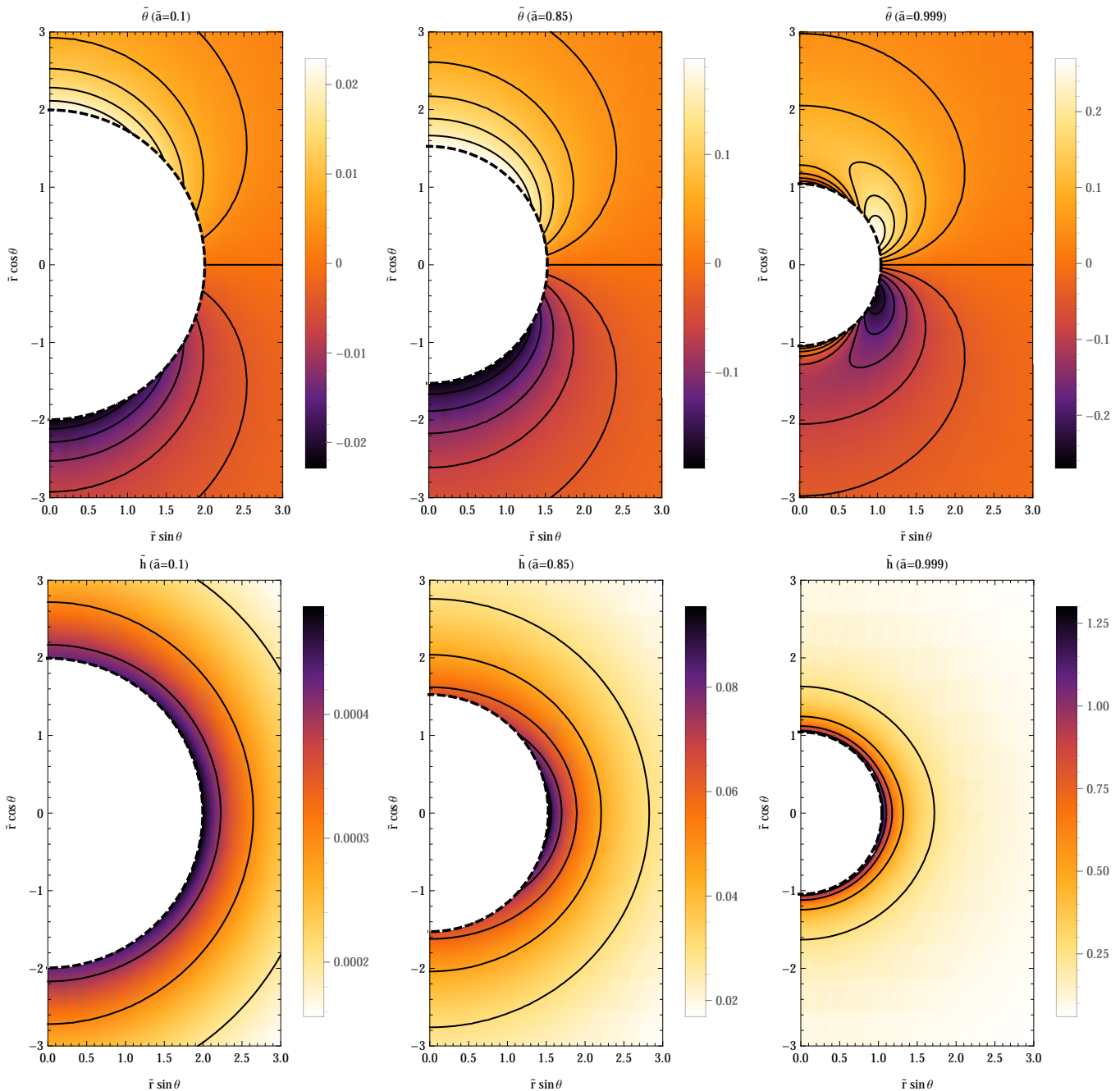


FIG. 3. (Color online) Profiles of solutions for $\tilde{\vartheta}$ (top panels) and \tilde{h} (bottom panels) in a longitudinal ($\phi = \text{const.}$) section of the space. From left to right, the profiles are at low spin ($\tilde{a} = 0.1$), intermediate ($\tilde{a} = 0.85$), and high spin ($\tilde{a} = 0.999$). Color represents the value of the field. Note the different color bar scale for each panel. Contours of constant field value are spaced linearly. The dashed line represents the horizon. At low spin, the $\tilde{\vartheta}$ solution is almost a pure dipole solution, $\propto P_1(\cos \theta)$. At intermediate and higher spin, the solutions develop more multipole structure. \tilde{h} is always highly peaked on the horizon at the equator, $\cos \theta = 0$. This is seen more easily in Fig. 4.

V. RESULTS AND DISCUSSION

We now turn to determining the regime of validity of the perturbation scheme. From Eq. (26), we see that we need to determine $\max |\tilde{h}(\tilde{a})|$. From the numerical scheme

described above, we see that \tilde{h} attains its maximum value on the horizon, at the equator. It is straightforward to extract this value from the numerical solutions. For this purpose we ran 29 models at different values of \tilde{a} , which takes about 5.5 sec on a laptop computer. We concentrated more models towards the endpoints ($\tilde{a} = 0$

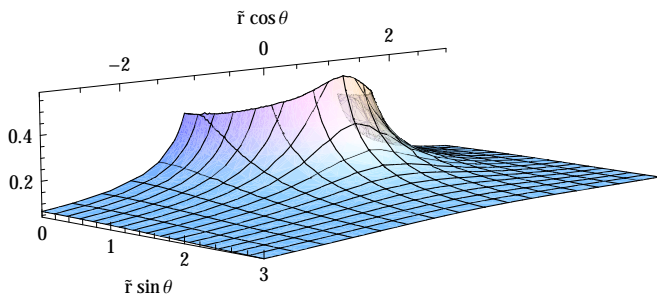


FIG. 4. (Color online) Surface representing the solution for \tilde{h} at $\tilde{a} = 0.99$ on a longitudinal ($\phi = \text{const.}$) section of the space. The two horizontal directions are $\tilde{r} \cos \theta$ and $\tilde{r} \sin \theta$ within the section, and the vertical height represents the value of $\tilde{h}(\tilde{r}, \theta)$. The solution peaks very strongly near the horizon. For all values of \tilde{a} , the maximum of \tilde{h} occurs on the equator at the horizon. This is the value which enters into Eq. (26) and thus the separatrix on Fig. 1.

and 1) where $\max|\tilde{h}(\tilde{a})|$ changes most rapidly with \tilde{a} . It is then simple to convert this to the separatrix between the regime of validity and breakdown through $|\ell/GM|^4 = 1/\max|\tilde{h}(a/GM)|$.

These results are presented in Fig. 1. As expected, larger values of \tilde{a} induce a larger Chern-Simons modification, and thus the range of ℓ/GM where the perturbation scheme is valid is smaller. The small- \tilde{a} behaviour can be easily understood analytically. Recall that for small spin, $\tilde{\vartheta} \propto \tilde{a}$, and then $\tilde{h} \propto \tilde{a}^2$. Taking the $-1/4$ power to convert to the ℓ -separatrix, we have that $|\ell/GM|_{\text{sep}} \propto \tilde{a}^{-1/2}$ for small \tilde{a} .

There is also clearly a feature at $\tilde{a} \rightarrow 1$. We do not have an analytic explanation for this feature, since analytic results are only available up to $\mathcal{O}(\tilde{a}^2)$ as a power series expansion, and we have no analytic expansion about $\tilde{a} \rightarrow 1$. Close examination of the maximum spin limit suggests that this limit may in fact be divergent. One possible explanation is as follows: Konno and Takahashi have suggested [16] that the scalar field solution blows up at the inner horizon. Recall that as $\tilde{a} \rightarrow 1$, the inner horizon approaches the outer horizon. This may lead to a divergence in $\tilde{\vartheta}$, and a worse divergence in \tilde{h} , since the source for \tilde{h} is constructed from $(\partial\tilde{\vartheta})^2$.

This strong spin dependence at the high-spin end has important implications for observationally constraining the coupling length ℓ . There are now several black hole systems known with spins approaching maximal values. One very promising candidate is GRO J1655-40, with a mass $M = 6.30 \pm 0.27 M_\odot$ and a spin $\tilde{a} \approx 0.65\text{--}0.75$ [28]. If it were observationally possible to infer that this system is well described everywhere by general relativity (i.e., that deviations from GR are small), then we could make the claim that

$$\ell \lesssim 15 GM_\odot \approx 22 \text{ km}. \quad (36)$$

Such a bound would improve on present Solar System constraints [29] by seven orders of magnitude, and is comparable in magnitude to that forecasted by [30]. We must caution the reader, though, that such bounds will be highly dependent on modeling of the physics of the accretion disk, which is uncertain.

Future work

As we have mentioned above, there are still several outstanding issues which warrant further investigation. We do not have an analytic explanation of the $\tilde{a} \rightarrow 1$ limit seen in Fig. 1. Just as it's possible to perform a slow-spin expansion, it should be possible to perform a near-extremal expansion to get a better understanding of this limit. Perhaps it is possible to obtain a fully analytic solution valid for all a .

The bounds we have forecasted here are just estimates, and real bounds would require much more work. Most important is an understanding of the impact of the dCS correction on the electromagnetic observables from BH binary systems, and how degenerate is the signature with modeling uncertainty of the accretion physics. This certainly requires a full metric solution, not just the trace.

Stepping back further, there is another regime of validity which we should discuss. Here we have concerned ourselves with the validity of the perturbation scheme for the decoupling limit. There is also the validity or breakdown of the effective field theory: the action is thought of as an ℓ expansion of some higher-energy theory, and we have truncated at some order. The two regimes of validity are not the same. A naïve estimate of the EFT breakdown is at $|\ell| \sim GM$, which does not involve spin at all. Note that at sufficiently high spin, the weak-coupling breakdown crosses the EFT breakdown. We hope to investigate how the EFT breakdown relates to our results.

ACKNOWLEDGMENTS

The author acknowledges Barry Wardell, Éanna Flanagan, David Nichols, Peter Taylor, Kent Yagi, and Nico Yunes for useful discussion. LCS acknowledges that support for this work was provided by the National Aeronautics and Space Administration through Einstein Postdoctoral Fellowship Award Number PF2-130101 issued by the Chandra X-ray Observatory Center, which is operated by the Smithsonian Astrophysical Observatory for and on behalf of the National Aeronautics Space Administration under contract NAS8-03060.

-
- [1] C. M. Will, *Living Reviews in Relativity* **17** (2014), 10.12942/lrr-2014-4, arXiv:1403.7377 [gr-qc].
- [2] S. Hawking, *Nature* **248**, 30 (1974).
- [3] A. Almheiri, D. Marolf, J. Polchinski, and J. Sully, *JHEP* **1302**, 062 (2013), arXiv:1207.3123 [hep-th].
- [4] S. L. Braunstein, S. Pirandola, and K. Życzkowski, *Phys.Rev.Lett.* **110**, 101301 (2013), arXiv:0907.1190 [quant-ph].
- [5] T. Jacobson, *Phys.Rev.Lett.* **75**, 1260 (1995), arXiv:gr-qc/9504004 [gr-qc].
- [6] T. Damour and G. Esposito-Farese, *Class.Quant.Grav.* **9**, 2093 (1992).
- [7] P. Kanti, N. E. Mavromatos, J. Rizos, K. Tamvakis, and E. Winstanley, *Phys.Rev.* **D54**, 5049 (1996), arXiv:hep-th/9511071 [hep-th].
- [8] C. de Rham, (2014), arXiv:1401.4173 [hep-th].
- [9] R. Jackiw and S. Y. Pi, *Phys.Rev.* **D68**, 104012 (2003), arXiv:gr-qc/0308071 [gr-qc].
- [10] S. Alexander and N. Yunes, *Phys.Rept.* **480**, 1 (2009), arXiv:0907.2562 [hep-th].
- [11] T. Delsate, D. Hilditch, and H. Witek, (2014), arXiv:1407.6727 [gr-qc].
- [12] N. Yunes and F. Pretorius, *Phys. Rev. D* **79**, 084043 (2009), arXiv:0902.4669 [gr-qc].
- [13] K. Konno, T. Matsuyama, and S. Tanda, *Prog.Theor.Phys.* **122**, 561 (2009), arXiv:0902.4767 [gr-qc].
- [14] P. Pani, C. F. B. Macedo, L. C. B. Crispino, and V. Cardoso, *Phys.Rev.* **D84**, 087501 (2011), arXiv:1109.3996 [gr-qc].
- [15] K. Yagi, N. Yunes, and T. Tanaka, *Phys.Rev.* **D86**, 044037 (2012), arXiv:1206.6130 [gr-qc].
- [16] K. Konno and R. Takahashi, (2014), arXiv:1406.0957 [gr-qc].
- [17] B. Kleihaus, J. Kunz, and E. Radu, *Phys.Rev.Lett.* **106**, 151104 (2011), arXiv:1101.2868 [gr-qc].
- [18] R. M. Wald, *General Relativity* (University of Chicago Press, 1984).
- [19] L. C. Stein and K. Yagi, *Phys.Rev.* **D89**, 044026 (2014), arXiv:1310.6743 [gr-qc].
- [20] B. A. Campbell, M. J. Duncan, N. Kaloper, and K. A. Olive, *Phys.Lett.* **B251**, 34 (1990).
- [21] S. Teukolsky, *Phys.Rev.Lett.* **29**, 1114 (1972).
- [22] S. A. Teukolsky, *Astrophys.J.* **185**, 635 (1973).
- [23] S. A. Teukolsky, *Perturbations of a rotating black hole*, Ph.D. thesis, California Institute of Technology (1974).
- [24] L. C. Stein, (2014), arXiv:1407.0744 [gr-qc].
- [25] A. C. Ottewill and P. Taylor, *Phys.Rev.* **D86**, 024036 (2012), arXiv:1205.5587 [gr-qc].
- [26] P. Taylor, personal communication (2013).
- [27] J. Boyd, *Chebyshev and Fourier Spectral Methods: Second Revised Edition*, Dover Books on Mathematics (Dover Publications, 2001).
- [28] R. Shafee, J. E. McClintock, R. Narayan, S. W. Davis, L.-X. Li, *et al.*, *Astrophys.J.* **636**, L113 (2006), arXiv:astro-ph/0508302 [astro-ph].
- [29] Y. Ali-Haïmoud and Y. Chen, *Phys.Rev.* **D84**, 124033 (2011), arXiv:1110.5329 [astro-ph.HE].
- [30] K. Yagi, N. Yunes, and T. Tanaka, *Phys.Rev.Lett.* **109**, 251105 (2012), arXiv:1208.5102 [gr-qc].